Polarization-dependent spectral broadening of femtosecond pulses in silicon waveguides

Chethiya M. Dissanayake,[1] Ivan D. Rukhlenko,[1,*] Malin Premaratne,[1] and Govind P. Agrawal[2]

[1]*Advanced Computing and Simulation Laboratory (AχL), Department of Electrical and Computer Systems Engineering, Monash University, Clayton, VIC 3800, Australia*
[2]*The Institute of Optics, University of Rochester, Rochester, New York 14627, USA*
*Corresponding author: ivan.rukhlenko@monash.edu

We investigate the polarization dependence of the spectral broadening of femtosecond pulses inside silicon waveguides by using finite-difference time-domain (FDTD) simulations. Our FDTD model includes the anisotropic dependency of predominant nonlinear effects in silicon: Kerr effect, two-photon absorption, and Raman effect. In addition, free-carrier absorption and free-carrier dispersion effects are incorporated into the model. The anisotropic nature of the silicon nonlinearities leads to the polarization-dependent spectral broadening of optical pulses inside silicon waveguides. Our study unambiguously shows that the spectral broadening inside silicon waveguides can be enhanced by carefully selecting the polarization angle of the input optical pulse. Numerical calculations reveal nearly a 4.5-times increase in spectral broadening (inside a 0.1 mm long silicon waveguide) when the polarization angle of the input pulse is adjusted accordingly. The combined impact of silicon nonlinearities and output polarizer on spectral broadening is investigated for different input polarization angles. Finally we show numerically that, for a given waveguide length and input peak intensity, there is an optimum pulse width that corresponds to the maximum spectral broadening.   © 2011 Optical Society of America

OCIS codes: 050.1755, 160.1190, 160.4330, 300.6170.

1. INTRODUCTION

The future of data communication rests on the ability to bring optical technologies from large-scale to chip-scale applications, in order to utilize the versatility of photon transportation at the processor level [1–3]. In fact, the integration of chip-scale photonics with electronics would combine the advantages of both technologies and uplift the performance of today's microprocessor to a new level of speed, while reducing the power consumption and physical size. Because of the unified fabrication framework, advantageous economies of scale could eventually lead to low-cost manufacturing of such integrated devices. Given that premise, silicon-on-insulator technology has attracted a great deal of interest in recent years, as it offers a promising platform for combining optical functionalities with electronics on a single substrate [4].

Because of the strong interaction of photons with electrons and phonons in silicon, a variety of optical phenomena are exhibited even within micrometer-sized silicon devices at moderate power levels [5,6]. However, the utilization of silicon optical phenomena in realizing photonic applications received little attention until the 1980s, due to a number of fundamental barriers in silicon [5]. Silicon is an indirect bandgap material, unlike the III-V compounds [7], which means that the light emission via electrical excitation in silicon is significantly weak. In addition, the second-order electro-optic effect, known as the Pockels effect, is absent in silicon due to the inverse symmetry of its crystalline lattice [8]. Consequently, modulation of electrical signal onto optical carriers in silicon had been a challenging task. Despite these issues, silicon is viewed as a potential material for manipulating light, after pioneering research carried out by Soref during the

1980s [9–11]. As a result, many of the basic components required in optical networking were demonstrated by using silicon photonics technology during the 1990s and later [12–14]. In addition, silicon photonics is motivated by the low cost and mass-scale manufacturing facilities of silicon microelectronics [15].

Among a plethora of silicon nonlinearities, the third-order effects are particularly significant because they give rise to a wide variety of optical phenomena [16–18]. Third-order nonlinearities in silicon have two major contributions: one from optical phonons and the other from bound electrons. The optical phonon contribution yields an inelastic scattering process of light known as stimulated Raman scattering (SRS) [19,20]. On the other hand, the real part of the electronic contribution corresponds to the Kerr effect, which gives rise to a number of interesting optical phenomena, including self-phase modulation (SPM), cross-phase modulation, third-harmonic generation, and four-wave mixing (FWM). The imaginary part of the electronic contribution corresponds to an absorption process referred to as two-photon absorption (TPA) [16,17]. By exploiting the dispersive and anisotropic properties of the third-order nonlinearities, a number of silicon photonic devices—such as all-optical Kerr shutters, power equalizers, and frequency converters—have been realized [21–23]. It is significant that the performance of most silicon photonic devices can be optimized by tailoring pulse polarization and waveguide orientation [24,25].

The exploitation of third-order nonlinearities in silicon to broaden the spectrum of optical pulses, also known as supercontinuum generation, has attracted much interest from the research community [26–28]. The ultrabroadband light sources are required in such applications as spectrum-sliced

WDM systems [29], optical coherence tomography [30], and high-precision metrology [31]. The SPM, FWM, and intrapulse Raman scattering are the main contributors to the spectral broadening in silicon waveguides [16,17]. Pulses propagating in the anomalous dispersion regime exhibit relatively larger (compared to the normal dispersion regime) spectral broadening, because the FWM process is enhanced with the phase matching condition [28]. Nonlinear absorption processes in silicon, TPA and free-carrier absorption (FCA), greatly reduce the efficiency of SPM and act, therefore, detrimentally on the spectral broadening [32,33]. Although the nonlinear spectral broadening in silicon waveguides is extensively studied both experimentally and theoretically [26–28,34–36], the influence of the anisotropy of the third-order optical nonlinearities on the spectral broadening has not been analyzed so far.

In this paper, we investigate the polarization-dependent spectral broadening of femtosecond Gaussian pulses using the recently developed finite-difference time-domain (FDTD) model for silicon waveguides [25]. This FDTD model takes into account SRS, Kerr effect, TPA, FCA, and free-carrier dispersion (FCD) effects in silicon. In addition, the anisotropy of the Raman, Kerr, and TPA effects in silicon is included in the model. We show that the state of polarization of the propagating pulse can be tailored to optimize the efficiency of spectral broadening.

2. FDTD FRAMEWORK FOR SILICON WAVEGUIDES

A number of linear and nonlinear optical effects affect the propagation of light inside silicon waveguides [16,37,38] and should be taken into account for precise modeling of light propagation through silicon waveguides. The dominant linear effects are dispersion, scattering at waveguide imperfections, and linear absorption. The major nonlinear effects in silicon are SRS, the Kerr effect (K), TPA, FCA, and FCD. The influences of these effects on the optical field inside silicon are generally described through material polarization models [17,20,39]. The algebraic sum of the polarization terms constitutes the total material polarization

$$\tilde{\mathbf{P}}(\omega) = \tilde{\mathbf{P}}_L + \tilde{\mathbf{P}}_{\mathrm{SRS}} + \tilde{\mathbf{P}}_K + \tilde{\mathbf{P}}_{\mathrm{TPA}} + \tilde{\mathbf{P}}_{\mathrm{FC}}, \tag{1}$$

where tildes represent the Fourier transforms and subscripts denote the abbreviations used to refer each effect. The last term accounts for the polarization contribution stemming from free carriers (FC), which comprises FCA and FCD effects.

A comprehensive description of electric (**E**) and magnetic (**H**) field evolution inside silicon waveguides is provided by source-free Maxwell's equations [40]

$$\nabla \times \mathbf{E} = -\mu_0 \frac{\partial \mathbf{H}}{\partial t}, \qquad \nabla \times \mathbf{H} = \varepsilon_0 \frac{\partial \mathbf{E}}{\partial t} + \frac{\partial \mathbf{P}}{\partial t}, \tag{2}$$

where μ_0 and ε_0 are the permeability and permittivity of a vacuum. One should comprehend the description of each polarization model in order to investigate solutions for Eq. (2). Therefore, the rest of the section is devoted to describing the polarization models of each optical effect in silicon.

Given that the effective refractive index is n_0 and the speed of light in a vacuum is c, the polarization contribution

from the linear optical effects in silicon waveguides is given by [41]

$$\tilde{\mathbf{P}}_L = \varepsilon_0 \left(-\frac{cn_0\alpha_L}{2i\omega} + \frac{a_1\omega_1^2}{\omega_1^2 - \omega^2} + \frac{a_2\omega_2^2}{\omega_2^2 - \omega^2} \right)\tilde{\mathbf{E}}, \tag{3}$$

where the first term accounts for linear absorption through the loss coefficient α_L. The second and third terms inside the brackets describe the linear dispersion of silicon. Assuming that the optical frequency of the propagating signal lies between 150 and 250 THz, the linear dispersion of silicon is described by the following parameters [28,42]: $a_1 = 9.733$, $a_2 = 0.936$, $\omega_1 = 1032.49\,\mathrm{THz}$, and $\omega_2 = 817.28\,\mathrm{THz}$.

In contrast to the linear responses, which are isotropic, the third-order nonlinear responses depend on the waveguide orientation and the state of polarization of the optical field. The mutual energy transfer between different frequency components of a light signal takes place due to the scattering of photons from optical phonons near the Brillouin zone center. This phenomenon is SRS [16,20,43]. The following classical model describes the SRS and is used in our FDTD algorithm [8,16]

$$\mathbf{P}_{\mathrm{SRS}}(t) = \varepsilon_0 \mathcal{R} \vdots \mathbf{E}(t) \int_{-\infty}^{t} H(t - t_1)\mathbf{E}(t_1)\mathbf{E}(t_1)\mathrm{d}t_1, \tag{4}$$

where three vertical dots indicate the product of tensor $\mathcal{R}$ with the three electric field vectors. The Fourier transform of the function $H(t)$ describes the Raman gain profile [16,43]

$$\tilde{H}(\omega) = \frac{2\xi_R \Omega_R \Gamma_R}{\Omega_R^2 - 2i\omega\Gamma_R - \omega^2},$$

where $\Omega_R = 15.6\,\mathrm{THz}$, $2\Gamma_R \approx 96\,\mathrm{GHz}$ is the gain linewidth [44], $\xi_R = 2\varepsilon_0 n_0 c^2 g_R/\omega_r$ with $\omega_r = 2\pi c/(1.55\,\mu\mathrm{m})$, and g_R is the Raman gain coefficient. The fourth-rank tensor $\mathcal{R}$ in Eq. (4) describes the anisotropy of the Raman scattering. In this study, we restrict our analysis to only the silicon waveguide fabricated along the [110] direction on the (001) plane (see Fig. 1). This is the most popular fabrication orientation of silicon waveguides due to the cleaving convenience [16,45]. We denote the cartesian FDTD axes x, y, and z along the [110], [$\bar{1}$10], and [001] directions, respectively. Adopted convention for the TE and TM polarization modes is shown in Fig. 1.
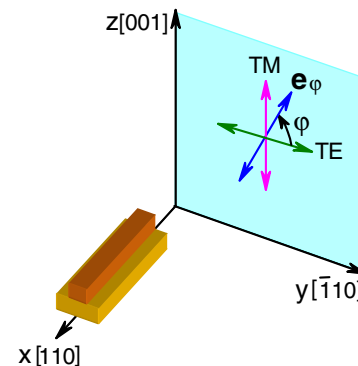

Fig. 1.   (Color online) Silicon waveguide fabricated along the [110] direction on the (001) plane. Axes x, y, and z are used in implementing the FDTD algorithm. The inset shows the TM and TE polarizations and an arbitrary linear polarization determined by the angle φ.

For this waveguide orientation, tensor $\mathcal{R}$ has the following nonzero components [25]:

$$xxxx = yyyy = -xxyy = -yyxx = xzxz = zxzx = xzzx$$
$$= zxxz = yzyz = zyzy = yzzy = zyyz = 1.$$

The Kerr effect originates from a direct polarization of the electronic clouds around silicon atoms caused by the optical field and has a typical response time in the femtosecond range. Since this time is comparable to the duration of an optical cycle, it is reasonable to assume the Kerr effect to be instantaneous. This assumption yields the Kerr-induced polarization of the form [16,17]

$$\mathbf{P}_K(t) = \varepsilon_0 \varepsilon_2 \mathcal{E} : \mathbf{E}(t)\mathbf{E}(t)\mathbf{E}(t), \tag{5}$$

where $\varepsilon_2 = \varepsilon_0 n_0^2 c n_2$ and n_2 is the Kerr coefficient. The anisotropy of the Kerr effect is characterized by the fourth-rank tensor $\mathcal{E}$, which has the following nonzero elements [8,16]:

$$xxxx = yyyy = (\rho + 1)/2, \qquad zzzz = 1,$$
$$xxyy = xyyx = yyxx = xyxy = yxyx = yxxy = (3 - \rho)/6,$$
$$xxzz = xzzx = zzxx = xzxz = zxzx = zxxz = yyzz = yzzy$$
$$= zzyy = yzyz = zyzy = zyyz = \rho/3,$$

where $\rho \approx 1.27$ near $\lambda = 1.55 \, \mu\mathrm{m}$.

The anisotropy of TPA is identical to that of the Kerr effect; this allows TPA-induced polarization to be written using the anisotropy tensor $\mathcal{E}$ as [25]

$$\tilde{\mathbf{P}}_{\mathrm{TPA}}(\omega) = -\frac{\varepsilon_0^2 c^2 n_0^2 \beta_{\mathrm{TPA}}}{2i\omega} \int_{-\infty}^{+\infty} \mathcal{E} : \mathbf{E}(t)\mathbf{E}(t)\mathbf{E}(t) e^{i\omega t} \mathrm{d}t, \tag{6}$$

where β_{TPA} is the TPA coefficient.

A large number of free carriers are generated through the process of TPA when two photons with energy $\hbar\omega_0$ exceed the bandgap of silicon. Assuming that the frequency of the absolute maximum of the input field spectrum is ω_0, the dynamics of those free carriers is governed by

$$\frac{\partial N(t)}{\partial t} = -\frac{N(t)}{\tau_c} + \frac{\beta_{\mathrm{TPA}}}{2\hbar\omega_0} \left(\frac{c\varepsilon_0 n_0 |\mathbf{E}(t)|^2}{2} \right)^2,$$

where $N(t)$ is the free-carrier density and τ_c is the effective free-carrier lifetime. Once created, free carriers interact with the propagating light by absorbing the energy of the light and by changing the refractive index of the waveguide. The former is referred to as FCA, while the later is referred to as FCD. The polarization model that accounts for these two FC effects is given by [16,17,39]

$$\tilde{\mathbf{P}}_{\mathrm{FC}}(\omega) = -\varepsilon_0 n_0 \left(\frac{c}{2i\omega} \sigma + \zeta \right) \left(\frac{\omega_r}{\omega_0} \right)^2 N \tilde{\mathbf{E}}, \tag{7}$$

and the terms inside the brackets account for FCA and FCD through the empirical coefficients $\sigma = 1.45 \times 10^{-21} \, \mathrm{m}^2$ and $\zeta = 5.3 \times 10^{-27} \, \mathrm{m}^3$, respectively.

The parts of Eq. (2) do not generally possess exact analytical solutions due to the complexity of the polarization term and the complicatedness of the photonic structures one has to deal with. Therefore, it is required to solve these equations numerically, using advanced computational techniques. The FDTD method is one of the most popular of such techniques for solving Maxwell's equation [46]; it discretizes the electromagnetic field components in the space and time domains according to the recipe proposed by Yee [47]. Applicability of the FDTD scheme for practical media has been drastically increased, as several research groups proposed advanced and efficient methods for incorporating the complex polarization models into the standard FDTD algorithm [39,48–50]. This enables a precise investigation of light interaction with complex materials that exhibit nonlinear and anisotropic optical responses. We have recently developed an extended FDTD algorithm, which is capable of handling the discussed nonlinear anisotropic effects in silicon [25]. The cartesian components of $\mathbf{H}$ are calculated through the previous values of the electromagnetic field quantities. Electric field components and polarization components are coupled together and solved iteratively until the results are converged. The full implementation of this extended FDTD algorithm can be found in Ref. [25].

Using the extended FDTD algorithm [25], we investigate the spectral broadening of femtosecond Gaussian pulses in silicon waveguides. Simulation results are provided in the next section.

3. RESULTS AND DISCUSSION

Owing to strong nonlinear effects in silicon, optical signals change their initial spectral widths as they propagate along silicon waveguides. For a detailed investigation of such spectral change, we simulate the propagation of femtosecond Gaussian pulses in short silicon waveguides within the normal dispersion regime. The waveguides are assumed to be fabricated along the [110] direction on the (001) surface (see Fig. 1) and have square cross sections with dimensions larger than the propagation wavelength. The parameter values employed in the simulations are as follows: $\alpha = 1 \, \mathrm{dB/cm}$, $\beta_{\mathrm{TPA}} = 0.9 \, \mathrm{cm/GW}$, $\varepsilon_2 = 1.72 \times 10^{-19} \, \mathrm{m}^2/\mathrm{V}^2$, $n_0 = 3.17$, $\tau_c = 1 \, \mathrm{ns}$, and $g_R = 76 \, \mathrm{cm/GW}$. The following expression yields the electric field of the fully polarized Gaussian pulses at the source:

$$\mathbf{E}(t) = \mathbf{e}_\varphi A \exp[-t^2/(2\sigma^2)] \cos(\omega_0 t), \tag{8}$$

where $\mathbf{e}_\varphi = \mathbf{e}_y \cos\varphi + \mathbf{e}_z \sin\varphi$ is the unit vector characterizing the polarization of the electric field, A is the peak amplitude of the Gaussian pulse, σ determines the FWHM of the time signal as $T_0 = 2\sigma\sqrt{\ln 2}$, and ω_0 is the carrier frequency that is set to be 177 THz in all simulations. The output polarizer is always set to be aligned with the input polarization angle (i.e., φ).

First we consider the propagation of a linearly polarized ($\varphi = 45°$) Gaussian pulse with $T_0 = 70 \, \mathrm{fs}$ and input peak intensity of 200 GW/cm^2. Numerically calculated spectra at the output of 0.1, 0.2, and 0.4 mm long silicon waveguides are shown in Fig. 2. Horizontal double arrows indicate the bandwidth at the −3 dB level from the peak value of each signal. As can be seen by the black double arrow, the −3 dB bandwidth of the input Gaussian pulse is ~6 THz. The SPM phenomenon plays an important role in nonlinear spectral broadening of intense optical pulses [28,51,52]. In addition to SPM, nonlinear phenomena of SRS and FWM contribute
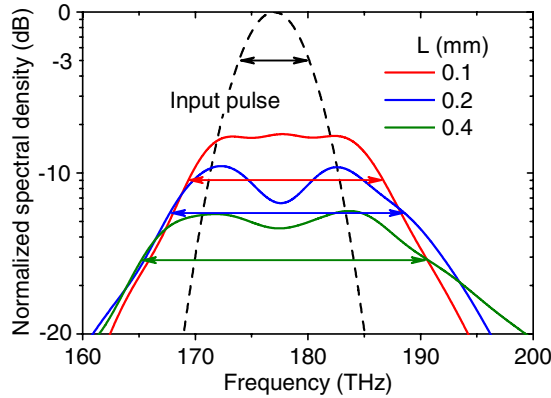
Fig. 2.   (Color online) Spectral broadening of 70 fs Gaussian pulse with input peak intensity of $200 \, \text{GW/cm}^2$ for different waveguide lengths L. Input polarization angle of the pulse is $\varphi = 45°$. Other parameter values are given in the text. Horizontal double arrows show the $-3 \, \text{dB}$ bandwidth of respective signals.

to the enhancement of the spectra of ultrashort pulses [53]. Since the effectiveness of these nonlinear phenomena increases with the propagating distance, one should expect larger spectral broadening from longer waveguides. The red curve in Fig. 2 shows the output spectra at the 0.1 mm waveguide, and it shows a nearly threefold increase of $-3 \, \text{dB}$ bandwidth compared to the input. The green curve, which corresponds to the spectrum at the output of the 0.4 mm waveguide, illustrates a nearly fourfold increase of $-3 \, \text{dB}$ bandwidth. The oscillatory behavior of the output spectrum is a result of SPM that manifests the same instantaneous frequency at two distinct points of the pulse. These two points have different phase values and cause constructive or destructive interference, leading to a multipeak structure in the output pulse spectrum [35,53].

In order to compare the efficiency of the bandwidth enhancement through waveguides, we define the following formula for the 3 dB spectral broadening S:

$$S = \frac{\Delta_{\text{out}}(-3 \, \text{dB}) - \Delta_{\text{in}}(-3 \, \text{dB})}{\Delta_{\text{in}}(-3 \, \text{dB})},$$

where $\Delta_{\text{out(in)}}(-3 \, \text{dB})$ is the $-3 \, \text{dB}$ bandwidth of the signal at the waveguide output (input).

To see how the input peak intensity of an optical pulse plays on the spectral broadening efficiency, we calculate S of a linearly polarized ($\varphi = 45°$) 70 fs Gaussian pulse for different input peak intensities. The results are illustrated in Fig. 3 for three different waveguide lengths. As mentioned earlier, since the optical nonlinearities are the dominant factors of spectral broadening in silicon waveguides, S increases with the pulse intensity and the propagation distance. According to the simulation results, a pulse with a $400 \, \text{GW/cm}^2$ input peak intensity shows $\sim 400\%$ spectral broadening at the output of a 0.4 mm silicon waveguide, while the same pulse shows only $\sim 250\%$ spectral broadening at the output of a 0.1 mm silicon waveguide. These results are in qualitative agreement with the results published in Ref. [35].

It is well known that the SPM arises through the Kerr and FCD effects. Since the Kerr effect in silicon is anisotropic, the amount of the SPM varies with the polarization of the optical field [23,24]. Consequently, the SPM-induced spectral broadening shows a polarization-dependent characteristic. In order
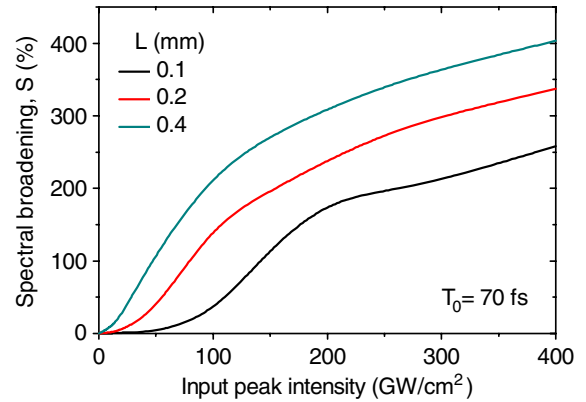

Fig. 3.   (Color online) Efficiency of spectral broadening of 70 fs Gaussian pulse as a function of input peak intensity for different waveguide lengths. Input polarization angle of the pulse is $\varphi = 45°$. Other parameter values are given in the text.

to investigate the influence of the input pulse polarization on the spectral broadening, we simulate the propagation of a 70 fs pulse through a 0.1 mm long silicon waveguide for different input polarization angles. First, we neglect the SRS effect in order to study the Kerr-induced spectral broadening and its anisotropic characteristics; the calculated S is shown by the red curve in Fig. 4. It is clearly seen that the TE mode ($\varphi = 0°$) exhibits larger spectral broadening than that in the TM mode ($\varphi = 90°$). The reason for this difference is that the Kerr-induced polarization is larger for the TE mode than for the TM mode by a factor of $(\rho + 1)/2 \approx 1.14$ [25]. It is also seen from the red curve that the maximum spectral broadening corresponds to the input polarization angle of $\varphi \approx 35°$. In order to explain this maximum spectral broadening, we consider the plane wave propagation along the x direction through a silicon waveguide fabricated as shown in Fig. 1. For such a situation, expanding Eq. (5), we can obtain y and z components of the Kerr-induced material polarization as

$$P_{Ky} = \varepsilon_0 \varepsilon_2 \left[\frac{(\rho + 1)}{2} E_y^2 + \rho E_z^2 \right] E_y,$$

$$P_{Kz} = \varepsilon_0 \varepsilon_2 (E_z^2 + \rho E_y^2) E_z.$$

Let us assume that the waveguide is sufficiently short such that the change in the state of the polarization is negligibly small. Thus, throughout the waveguide
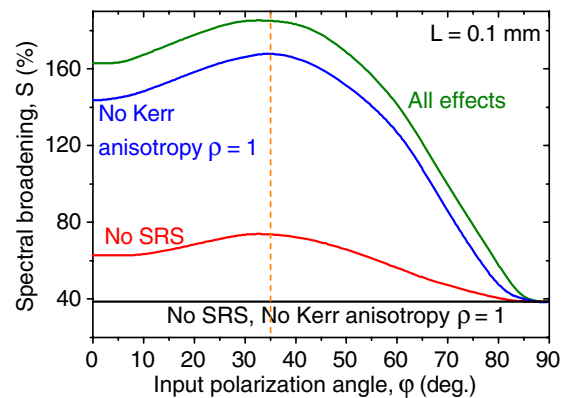

Fig. 4.   (Color online) Spectral broadening of 70 fs Gaussian pulse for different input polarization angles. Input peak intensity of the pulse is $200 \, \text{GW/cm}^2$, and the silicon waveguide is 0.1 mm long.

$$\frac{E_z(t)}{E_y(t)} = \tan\varphi, \tag{9}$$

where φ is the input polarization angle. Now we introduce an axillary term $G(t)$ as

$$E_y^2(t) + E_z^2(t) = G(t). \tag{10}$$

It should be noted that $G(t)$ constitutes the power profile of the pulse, and it is independent of the input polarization angle. Using Eqs. (9) and (10), we can express electric field components in terms of $G(t)$ and φ as

$$E_y(t) = \sqrt{\frac{G(t)}{1+\tan^2\varphi}}, \qquad E_z(t) = \sqrt{\frac{G(t)}{1+\tan^2\varphi}}\tan\varphi.$$

The use of these expressions in obtaining the input polarization dependence of Kerr polarization leads to

$$|\mathbf{P}_K(t)|$$
$$= \varepsilon_0\varepsilon_2 G^{3/2}(t)\frac{\sqrt{\tan^2\varphi(\rho+\tan^2\varphi)^2 + [(\rho+1)/2 + \rho\tan^2\varphi]^2}}{(1+\tan^2\varphi)^{3/2}}.$$

This function has its maximum at $\varphi = \tan^{-1}(1/\sqrt{2}) \approx 35.3°$; hence, the SPM-induced spectral broadening is maximum for optical pulses polarized at $\varphi \approx 35.3°$.

In addition to the Kerr effect, the Raman scattering also contributes to the spectral broadening, provided that the pulse is much shorter than the Raman response time of 3 ps [16]. Expanding Eq. (4) for plane waves that propagate along the x direction, one can obtain the y and z components of the Raman-induced polarization as

$$P_{\mathrm{SRS}y} = \varepsilon_0\left[E_y\int_{-\infty}^{t}H(t-t_1)E_y^2\mathrm{d}t_1 + E_z\int_{-\infty}^{t}H(t-t_1)E_yE_z\mathrm{d}t_1\right.$$
$$\left. + E_z\int_{-\infty}^{t}H(t-t_1)E_zE_y\mathrm{d}t_1\right],$$
$$P_{\mathrm{SRS}z} = \varepsilon_0\left[E_y\int_{-\infty}^{t}H(t-t_1)E_yE_z\mathrm{d}t_1 + E_y\int_{-\infty}^{t}H(t-t_1)E_zE_y\mathrm{d}t_1\right].$$

For short waveguides, employing the relationships stated in Eqs. (9) and (10), the above polarization components can be rewritten as

$$P_{\mathrm{SRS}y} = \varepsilon_0\sqrt{G(t)}\frac{(1+2\tan^2\varphi)}{(1+\tan^2\varphi)^{3/2}}I(t),$$
$$P_{\mathrm{SRS}z} = \varepsilon_0\sqrt{G(t)}\frac{2\tan\varphi}{(1+\tan^2\varphi)^{3/2}}I(t),$$

where $I(t) = \int_{-\infty}^{t}H(t-t_1)G(t_1)\mathrm{d}t_1$. Now we can state the Raman-induced polarization as a function of φ as follows:

$$|\mathbf{P}_{\mathrm{SRS}}(t)| = \varepsilon_0\sqrt{G(t)}I(t)\frac{\sqrt{(1+2\tan^2\varphi)^2+4\tan^2\varphi}}{(1+\tan^2\varphi)^{3/2}}.$$

This function has its maximum at $\varphi = \tan^{-1}(1/\sqrt{2}) \approx 35.3°$. Therefore, the blue curve in Fig. 4 shows its maximum for this input polarization angle. It is well known that the Raman scattering is absent for the TM mode [16,25,43,45]; this is the
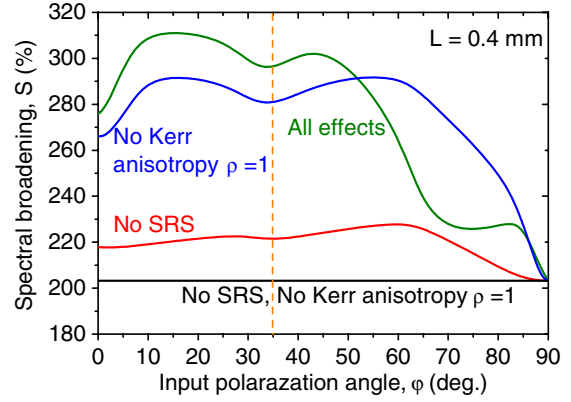

Fig. 5. (Color online) Spectral broadening of 70 fs Gaussian pulse for different input polarization angles. Input peak intensity of the pulse is $200\,\mathrm{GW/cm}^2$, and the silicon waveguide is 0.4 mm long.

reason for the minimal spectral broadening for input polarization angle $\varphi = 90°$ (see the blue curve in Fig. 4). The green curve shows the spectral broadening when all the nonlinear effects (i.e., SRS, Kerr, TPA, FCA, and FCD) in silicon are taken into account. The maximum spectral broadening (corresponding to $\varphi \approx 35.3°$) in this curve shows a spectral broadening enhancement of nearly 4.5 times compared to the TM mode.

As a result of the anisotropic nature of the Kerr, TPA, and Raman effects, the state of polarization of the pulse rotates as it propagates along the silicon waveguide [24,25]. If a polarizer is placed at the end of the waveguide, the output signal experiences an additional wave shaping because the electromagnetic field that is perpendicular to the polarizer is clipped off [25]. This situation—caused by the polarization rotation and the output polarizer—contributes to a further enhancement of the spectrum of the output signal. Therefore, in addition to the nonlinearity-induced spectral broadening, the polarization rotation and output polarizer effect should be considered in explaining the total spectral broadening, particularly in longer waveguides. The red curve in Fig. 5 shows the spectral broadening of 70 fs pulses at the output of a 0.4 mm long silicon waveguide when Raman scattering is neglected. In contrast to the results obtained for a 0.1 mm long waveguide (Fig. 4), the maximum spectral broadening does not correspond to the input polarization angle $\varphi \approx 35.3°$. Indeed, the peak of the spectral broadening is evident near
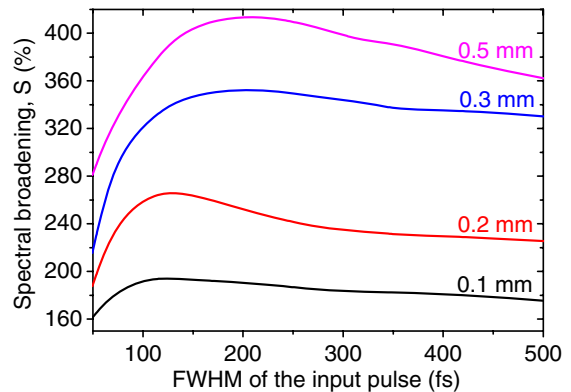

Fig. 6. (Color online) Spectral broadening of Gaussian pulse with different pulse widths. Pulse peak intensity is $200\,\mathrm{GW/cm}^2$. Input pulse polarization is $\varphi \approx 45°$.

$\varphi \approx 60°$. This situation can be described as follows: unlike the shorter waveguides, for longer waveguides, the polarization rotation is an important phenomenon, and hence the combined influence of nonlinearities and the output polarizer effect contributes to the spectral broadening. It should be noted that for a given waveguide length, the extent of polarization rotation depends on the input polarization angle of the pulse [24,25]. Pulses preserve their initial polarization state when they propagate in either TE mode, TM mode, or a mode determined by the polarization angle $\varphi = \tan^{-1}(1/\sqrt{2}) \approx 35.3°$ [25]. In addition, the largest amount of polarization rotation is reported to take place for input polarization angle $\varphi \approx 60°$ [25]. Therefore, the largest extent of spectral broadening is shown when $\varphi \approx 60°$, but not when $\varphi \approx 35.3°$. Moreover, the effect of TPA is maximum for $\varphi \approx 35.3°$, because TPA possesses the same anisotropy as the Kerr effect. It is a well-known fact that the TPA process limits the spectral broadening in silicon waveguides [33,35,36]. Since the TPA accumulates with the propagating distance, for longer waveguides the spectral broadening at $\varphi \approx 35.3°$ becomes weaker. This is the reason for the slight dip in the red curve at $\varphi \approx 35°$.

The polarization rotation due to Raman scattering has similar characteristics to those of Kerr-induced polarization rotation. This means that the Raman-induced spectral broadening shows local maxima when the polarization angle is either $\varphi \approx 15°$ or $\varphi \approx 60°$. The respective minima are at $\varphi = 0°$, $\varphi = 90°$, and $\varphi = \tan^{-1}(1/\sqrt{2}) \approx 35.3°$. It is important to note that when all effects are included (see the green curve in Fig. 5), the maximum near $\varphi \approx 60°$ disappears. The reason for this is the joint impact of the Raman and Kerr effects, which tend to cancel each other for $\varphi \geq \tan^{-1}(1/\sqrt{2}) \approx 35.3°$.

Finally, we investigate the efficiency of the spectral broadening for different pulse widths. Figure 6 illustrates the calculated S for a linearly polarized ($\varphi = 45°$) Gaussian pulse with a $200\,\text{GW/cm}^2$ input peak intensity. It is clearly seen from the figure that for a given waveguide length, there is an optimum pulse width that gives the maximum spectral broadening. For example, the spectral broadening at the end of a 0.2 mm silicon waveguide is maximum for pulse width ~120 fs. The reason for this is the interplay between the Raman and free-carrier effects. For shorter pulses the Raman effect becomes the dominant effect contributing to the spectral broadening, and free-carrier effects on spectral broadening become weaker. For longer pulses, the Raman effect becomes weaker, and free-carrier effects strongly contribute to the broadening of spectra. The optimum pulse width corresponds to the maximum aggregate of the Raman and free-carrier effects on spectral broadening.

4. CONCLUSIONS

We have simulated the propagation of femtosecond Gaussian pulses inside silicon waveguides by using an extended FDTD scheme that takes into account the anisotropy of the Kerr, TPA, and Raman effects. A detailed numerical investigation was carried out to characterize the dependency of the input polarization of optical pulses on spectral broadening. Owing to the inherent coupling between dispersion and nonlinearity, silicon gives rise to substantial spectral broadening even in submillimeter scale waveguides. The impact of optical nonlinearities increases with the input intensity of signal; therefore, the pulses with a larger input intensity exhibit greater spectral broadening. Moreover, according to the simulation results, the spectral broadening can be enhanced by launching the input signal at the polarization angle of $\varphi \approx 35.3°$, because the impacts of both Kerr and Raman effects are maximized at this mode. For longer waveguides, where the polarization rotation is substantial, the spectral broadening is a combined outcome of the nonlinearity-induced self-phase modulation and the output polarizer effect. Furthermore, we have shown that for a given silicon waveguide, there is an optimal pulse width that gives the maximum spectral broadening.

REFERENCES

1. D. A. B. Miller, "Rationale and challenges for optical interconnects to electronic chips," Proc. IEEE **88**, 728–749 (2000).
2. N. Savage, "Linking with light (high-speed optical interconnects)," IEEE Spectrum **39**, 32–36 (2002).
3. B. Jalali, "Can silicon change photonics?" Phys. Status Solidi A **205**, 213–224 (2008).
4. U. Hilleringmann and K. Goser, "Optoelectronic system integration on silicon: waveguides, photodetectors, and VLSI CMOS circuits on one chip," IEEE Trans. Electron Devices **42**, 841–846 (1995).
5. R. A. Soref, "The past, present, and future of silicon photonics," IEEE J. Sel. Top. Quantum Electron. **12**, 1678–1687 (2006).
6. G. T. Reed and A. P. Knight, *Silicon Photonics: an Introduction* (Wiley, 2004).
7. I. Vurgaftman, J. R. Meyer, and L. R. Ram-Mohan, "Band parameters for III–V compound semiconductors and their alloys," J. Appl. Phys. **89**, 5815–5875 (2001).
8. R. W. Boyd, *Nonlinear Optics*, 2nd ed. (Academic, 2003).
9. R. A. Soref and J. P. Lorenzo, "Single-crystal silicon: a new material for 1.3 and 1.6 μm integrated-optical components," Electron. Lett. **21**, 953–954 (1985).
10. R. A. Soref and J. P. Lorenzo, "All-silicon active and passive guided-wave components for $\lambda = 1.3$ and 1.6 μm," IEEE J. Quantum Electron. **22**, 873–879 (1986).
11. R. A. Soref and B. Bennett, "Electrooptical effects in silicon," IEEE J. Quantum Electron. **23**, 123–129 (1987).
12. P. D. Trinh, S. Yegnanarayanan, and B. Jalali, "Integrated optical directional couplers in silicon-on-insulator," Electron. Lett. **31**, 2097–2098 (1995).
13. B. Jalali, S. Yegnanarayanan, T. Yoon, T. Yoshimoto, I. Rendina, and F. Coppinger, "Advances in silicon-on-insulator optoelectronics," IEEE J. Sel. Top. Quantum Electron. **4**, 938–947 (1998).
14. B. Jalali and S. Fathpour, "Silicon photonics," J. Lightwave Technol. **24**, 4600–4615 (2006).
15. H. Iwai and S. Ohmi, "Silicon integrated circuit technology from past to future," Microelectron. Reliability **42**, 465–491 (2002).
16. Q. Lin, O. J. Painter, and G. P. Agrawal, "Nonlinear optical phenomena in silicon waveguides: modeling and applications," Opt. Express **15**, 16604–16644 (2007).
17. R. M. Osgood Jr., N. C. Panoiu, J. I. Dadap, X. Liu, X. Chen, I. Hsieh, E. Dulkeith, W. M. J. Green, and Y. A. Vlasov, "Engineering nonlinearities in nanoscale optical systems: physics and applications in dispersion-engineered silicon nanophotonic wires," Adv. Opt. Photon. **1**, 162–235 (2009).
18. J. Leuthold, C. Koos, and W. Freude, "Nonlinear silicon photonics," Nat. Photon. **4**, 535–544 (2010).

19. R. Claps, D. Dimitropoulos, V. Raghunathan, Y. Han, and B. Jalali, "Observation of stimulated Raman amplification in silicon waveguides," Opt. Express **11**, 1731–1739 (2003).

20. X. Chen, N. C. Panoiu, and R. M. Osgood Jr., "Theory of Raman-mediated pulsed amplification in silicon-wire waveguides," IEEE J. Quantum Electron. **42**, 160–170 (2006).

21. J. Y. Lee, L. Yin, G. P. Agrawal, and P. M. Fauchet, "Ultrafast optical switching based on nonlinear polarization rotation in silicon waveguides," Opt. Express **18**, 11514–11523 (2010).

22. L. Yin, J. Zhang, P. M. Fauchet, and G. P. Agrawal, "Optical switching using nonlinear polarization rotation inside silicon waveguides," Opt. Lett. **34**, 476–478 (2009).

23. I. D. Rukhlenko, I. L. Garanovich, M. Premaratne, A. A. Sukhorukov, G. P. Agrawal, and Yu. S. Kivshar, "Polarization rotation in silicon waveguides: analytical modeling and applications," IEEE Photon. J. **2**, 423–435 (2010).

24. B. A. Daniel and G. P. Agrawal, "Vectorial nonlinear propagation in silicon nanowire waveguides: polarization effects," J. Opt. Soc. Am. B **27**, 956–965 (2010).

25. C. M. Dissanayake, M. Premaratne, I. D. Rukhlenko, and G. P. Agrawal, "FDTD modeling of anisotropic nonlinear optical phenomena in silicon waveguides," Opt. Express **18**, 21427–21448 (2010).

26. Ö. Boyraz, P. Koonath, V. Raghunathan, and B. Jalali, "All optical switching and continuum generation in silicon waveguides," Opt. Express **12**, 4094–4102 (2004).

27. I.-W. Hsieh, X. Chen, X. Liu, J. I. Dadap, N. C. Panoiu, C.-Y. Chou, F. Xia, W. M. Green, Y. A. Vlasov, and R. M. Osgood, "Supercontinuum generation in silicon photonic wires," Opt. Express **15**, 15242–15249 (2007).

28. L. Yin, Q. Lin, and G. P. Agrawal, "Soliton fission and supercontinuum generation in silicon waveguides," Opt. Lett. **32**, 391–393 (2007).

29. A. Liu, L. Liao, Y. Chetrit, J. Basak, H. Nguyen, D. Rubin, and M. Paniccia, "Wavelength division multiplexing based photonic integrated circuits on silicon-on-insulator platform," IEEE J. Sel. Top. Quantum Electron. **16**, 23–32 (2010).

30. W. Drexler, "Ultrahigh-resolution optical coherence tomography," J. Biomed. Opt. **9**, 47–74 (2004).

31. P. E. Murphy, J. Fleig, G. Forbes, and M. Tricard, "High precision metrology of domes and aspheric optics," Proc. SPIE **5786**, 112–121 (2005).

32. L. Yin and G. P. Agrawal, "Impact of two-photon absorption on self-phase modulation in silicon waveguides," Opt. Lett. **32**, 2031–2033 (2007).

33. Y. Liu, C. W. Chow, H. K. Tsang, and S. P. Wong, "Enhancement of self phase modulation induced spectral broadening in silicon waveguides by ion implantation," in *Conference on Lasers and Electro-Optics/Quantum Electronics and Laser Science Conference and Photonic Applications Systems Technologies*, OSA Technical Digest Series (CD) (Optical Society of America, 2007), paper CThQ2.

34. G. W. Rieger, K. S. Virk, and J. F. Young, "Nonlinear propagation of ultrafast 1.5 μm pulses in high-index-constrast silicon-on-insulator waveguides," Appl. Phys. Lett. **84**, 900–902 (2004).

35. Ö. Boyraz, T. Indukuri, and B. Jalali, "Self phase modulation induced spectral broadening in silicon waveguides," in *Conference on Lasers and Electro-Optics/International Quantum Electronics Conference and Photonic Applications Systems Technologies*, Technical Digest (CD) (Optical Society of America, 2004), paper CThJ2.

36. Ö. Boyraz, T. Indukuri, and B. Jalali, "Self-phase-modulation induced spectral broadening in silicon waveguides," Opt. Express **12**, 829–834 (2004).

37. I. D. Rukhlenko, M. Premaratne, and G. P. Agrawal, "Nonlinear silicon photonics: analytical tools," IEEE J. Sel. Top. Quantum Electron. **16**, 200–215 (2010).

38. I. D. Rukhlenko, M. Premaratne, C. M. Dissanayake, and G. P. Agrawal, "Nonlinear pulse evolution in silicon waveguides: an approximate analytic approach," J. Lightwave Technol. **27**, 3241–3248 (2009).

39. N. Suzuki, "FDTD analysis of two-photon absorption and free-carrier absorption in Si high-contrast waveguides," J. Lightwave Technol. **25**, 2495–2501 (2007).

40. M. Born and E. Wolf, *Principles of Optics*, 7th ed. (Cambridge University, 1999).

41. B. Tatian, "Fitting refractive-index data with the Sellmeier dispersion formula," Appl. Opt. **23**, 4477–4485 (1984).

42. C. M. Dissanayake, I. D. Rukhlenko, M. Premaratne, and G. P. Agrawal, "Raman-mediated nonlinear interactions in silicon waveguides: copropagating and counterpropagating pulses," IEEE Photon. Technol. Lett. **21**, 1372–1374 (2009).

43. B. Jalali, V. Raghunathan, D. Dimitropoulos, and Ö. Boyraz, "Raman-based silicon photonics," IEEE J. Sel. Top. Quantum Electron. **12**, 412–421 (2006).

44. Y. Okawachi, M. A. Foster, J. E. Sharping, A. L. Gaeta, Q. Xu, and M. Lipson, "All-optical slow-light on a photonic chip," Opt. Express **14**, 2317–2322 (2006).

45. A. Liu, H. Rong, R. Jones, O. Cohen, D. Hak, and M. Paniccia, "Optical amplification and lasing by stimulated Raman scattering in silicon waveguides," J. Lightwave Technol. **24**, 1440–1455 (2006).

46. A. Taflove and S. C. Hagness, *Computational Electrodynamics: the Finite-Difference Time-Domain Method*, 3rd ed. (Artech House, 2005).

47. K. S. Yee, "Numerical solution of initial boundary value problems involving Maxwell's equations in isotropic media," IEEE Trans. Antennas Propag. **14**, 302–307 (1966).

48. R. M. Joseph and A. Taflove, "FDTD Maxwell's equations models for nonlinear electrodynamics and optics," IEEE Trans. Antennas Propag. **45**, 364–374 (1997).

49. F. L. Teixeira, "Time-domain finite-difference and finite-element methods for Maxwell equations in complex media," IEEE Trans. Antennas Propag. **56**, 2150–2166 (2008).

50. J. Schneider and S. Hudson, "A finite-difference time-domain method applied to anisotropic material," IEEE Trans. Antennas Propag. **41**, 994–999 (1993).

51. H. K. Tsang, C. S. Wong, T. K. Liang, I. E. Day, S. W. Roberts, A. Harpin, J. Drake, and M. Asghari, "Optical dispersion, two-photon absorption and self-phase modulation in silicon waveguides at 1.5 μm wavelength," Appl. Phys. Lett. **80**, 416–418 (2002).

52. S. Roy, S. K. Bhadra, and G. P. Agrawal, "Femtosecond pulse propagation in silicon waveguides: variational approach and its advantages," Opt. Commun. **281**, 5889–5893 (2008).

53. G. P. Agrawal, *Nonlinear Fiber Optics*, 4th ed. (Academic, 2007).